

Journal Pre-proofs

Heteroarylamine Smoothened Inhibitors: Discovery of N-[2,4-dimethyl-5-(1-methylimidazol-4-yl)phenyl]-4-(2-pyridylmethoxy)benzamide (AZD8542) and N-[5-(1H-imidazol-2-yl)-2,4-dimethyl-phenyl]-4-(2-pyridylmethoxy)benzamide (AZD7254)

Bin Yang, Alexander W. Hird, Michael S. Bodnarchuk, Xiaolan Zheng, Les Dakin, Qibin Su, Kevin Daly, Robert Godin, Maureen M. Hattersley, Patrick Brassil, Sean Redmond, Daniel John Russell, James W. Janetka

PII: S0968-0896(19)30668-6
DOI: <https://doi.org/10.1016/j.bmc.2019.115227>
Reference: BMC 115227

To appear in: *Bioorganic & Medicinal Chemistry*

Received Date: 23 April 2019
Revised Date: 9 November 2019
Accepted Date: 14 November 2019

Please cite this article as: B. Yang, A.W. Hird, M.S. Bodnarchuk, X. Zheng, L. Dakin, Q. Su, K. Daly, R. Godin, M.M. Hattersley, P. Brassil, S. Redmond, D. John Russell, J.W. Janetka, Heteroarylamine Smoothened Inhibitors: Discovery of N-[2,4-dimethyl-5-(1-methylimidazol-4-yl)phenyl]-4-(2-pyridylmethoxy)benzamide (AZD8542) and N-[5-(1H-imidazol-2-yl)-2,4-dimethyl-phenyl]-4-(2-pyridylmethoxy)benzamide (AZD7254), *Bioorganic & Medicinal Chemistry* (2019), doi: <https://doi.org/10.1016/j.bmc.2019.115227>

This is a PDF file of an article that has undergone enhancements after acceptance, such as the addition of a cover page and metadata, and formatting for readability, but it is not yet the definitive version of record. This version will undergo additional copyediting, typesetting and review before it is published in its final form, but we are providing this version to give early visibility of the article. Please note that, during the production process, errors may be discovered which could affect the content, and all legal disclaimers that apply to the journal pertain.

© 2019 Published by Elsevier Ltd.



Heteroarylamide Smoothened Inhibitors: Discovery of N-[2,4-dimethyl-5-(1-methylimidazol-4-yl)phenyl]-4-(2-pyridylmethoxy)benzamide (AZD8542) and N-[5-(1H-imidazol-2-yl)-2,4-dimethyl-phenyl]-4-(2-pyridylmethoxy)benzamide (AZD7254)

Bin Yang,^{1*} Alexander W. Hird,¹ Michael S. Bodnarchuk,² Xiaolan Zheng,¹ Les Dakin,¹ Qibin Su,¹ Kevin Daly,¹ Robert Godin,³ Maureen M. Hattersley,³ Patrick Brassil,⁴ Sean Redmond,⁵ Daniel John Russell,¹ James W. Janetka^{1, †}

¹*Medicinal Chemistry, Oncology, IMED Biotech Unit, AstraZeneca, 35 Gatehouse Drive, Waltham MA 02451, USA*

²*Medicinal Chemistry, Oncology, IMED Biotech Unit, AstraZeneca, Building 310, Cambridge Science Park, Milton Road, Cambridge UK*

³*Bioscience, Oncology, IMED Biotech Unit, AstraZeneca, 35 Gatehouse Drive, Waltham MA 02451, USA*

⁴*Drug Metabolism and Pharmacokinetics, Oncology, IMED Biotech Unit, AstraZeneca, 35 Gatehouse Drive, Waltham MA 02451, USA*

⁵*Oncology Safety, Drug Safety and Metabolism, IMED Biotech Unit, AstraZeneca, 35 Gatehouse Drive, Waltham MA 02451, USA*

ABSTRACT

Aberrant hedgehog (Hh) pathway signaling is implicated in multiple cancer types and targeting the Smoothened (SMO) receptor, a key protein of the Hh pathway, has proven effective in treating metastasized basal cell carcinoma. Our lead optimization effort focused on a series of heteroarylamides. We observed that a methyl substitution *ortho* to the heteroaryl groups on an aniline core significantly improved the potency of this series of compounds. These findings predated the availability of SMO crystal structure in 2013. Here we retrospectively applied quantum mechanics calculations to demonstrate the *o*-Me substitution favors the bioactive conformation by inducing a

dihedral twist between the heteroaryl rings and the core aniline. The *o*-Me also makes favorable hydrophobic interactions with key residue side chains in the binding pocket. From this effort, two compounds (AZD8542 and AZD7254) showed excellent pharmacokinetics across multiple preclinical species and demonstrated *in vivo* activity in abrogating the Hh paracrine pathway as well as anti-tumor effects.

INTRODUCTION

The Hedgehog (Hh) pathway is a critical pathway during embryogenesis where it mediates cell proliferation, differentiation, and patterning of the embryo. This pathway has been conserved through evolution and has been identified throughout the animal kingdom including sea urchins, worms, flies and mammals.¹ The human genome contains three Hh genes, Sonic (SHH), Indian (IHH) and Desert (DHH). Hh proteins are secreted from the cell and bind a transmembrane receptor Ptch1. The function of Ptch1 is to inhibit a 7-pass membrane protein smoothed (SMO), a frizzled family G protein-coupled receptor (GPCR) that transmits the Hh signal across the membrane to the cytoplasm.² Multiple SMO inhibitors have been identified, including vismodegib (**1**),³ sonidegib (**2**),⁴ glasdegib (**3**),⁵⁻⁶ and taladegib (**4**)⁷ (**Figure 1**) and have been evaluated in clinical trials. Compounds **1** and **2** have been approved for the treatment of Basal Cell Carcinoma.⁸⁻⁹ Recently, renewed attention to Hh pathway inhibitors has been inspired after the X-ray structures of SMO became available.^{10,11,12} These recent breakthroughs in structural biology helped elucidate a mechanism where a large extracellular region and two allosterically linked ligand-binding sites in SMO regulate its activity. Cholesterol likely functions as an endogenous SMO ligand that binds to one of the two allosteric sites and stabilizes SMO to a resting or *apo* conformation poised to respond to Hh signals. SMO inhibitors, such as vismodegib, bind to the second allosteric site to occlude the cholesterol-binding site, inhibiting Hh signaling activity.¹² A more recent report suggests that known SMO inhibitors (e.g., cyclopamine and vismodegib) bind in and block a transmembrane hydrophobic

channel that could be used by the protein to shuttle cholesterol from the inner membrane to the extracellular Cysteine-Rich-Domain (CRD) in order to activate SMO.¹³ We previously disclosed a series heteroarylamides as potent SMO inhibitors with good preclinical pharmacokinetic profiles.¹⁴ Further optimization on this heteroarylamide series revealed some intriguing structure-activity relationships (SAR). Herein we report our work on these potent SMO inhibitors that was done before the availability of X-ray crystal structure of SMO. With the available ligand-bound crystal structures of SMO in the public domain, we also attempted to understand the observed SAR of these heteroarylamides in a retrospective sense.

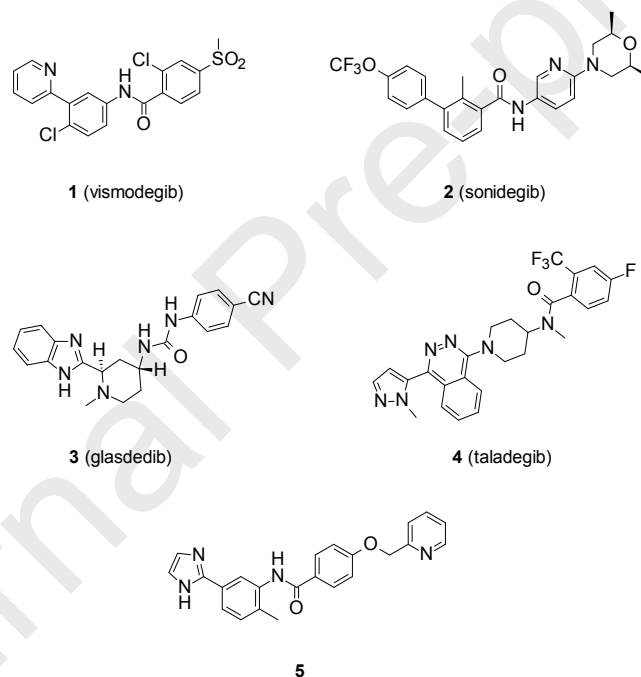


Figure 1. Structures of SMO inhibitors

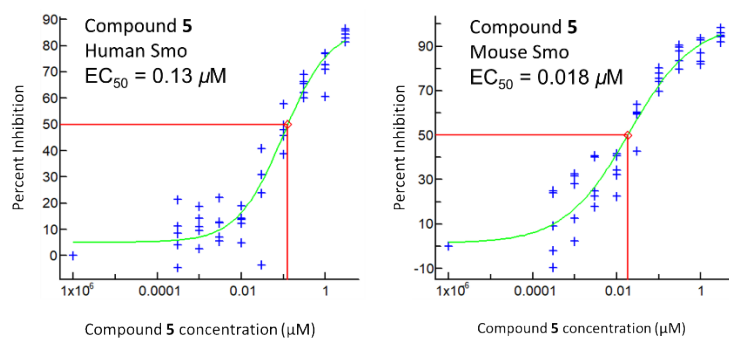
RESULTS AND DISCUSSION

GLI modulation and efficacy in mouse xenograft models.

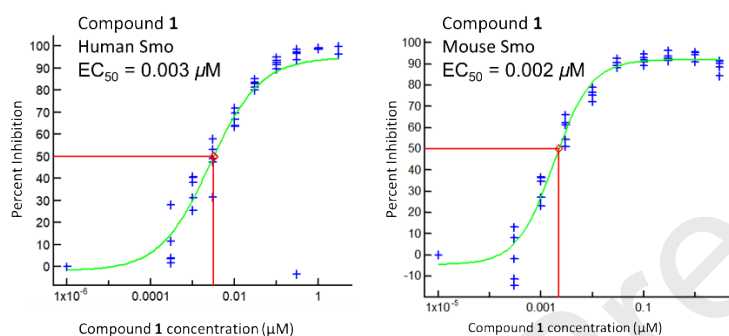
We previously reported compound **5** as a potent SMO inhibitor with excellent rodent PK and good physical properties.¹⁴ Compound **5** was further taken into *in vivo* studies and it demonstrated a dose

dependent pharmacologic effect (mouse GLI suppression) in both Colo2015 and NCI-H460 xenograft models (**Figures S1 and S2**). Although we observed reduced GLI expression in mouse stroma cells within the xenograft, no significant modulation of human GLI was observed in the tumour cells (**Figure S2 and Table S2**). Others have shown that activation of the Hh pathway by SHH does not affect endogenous GLI1 mRNA levels in tumor epithelial cells (Bxpc3 and CFPAC-1), and suggested that Hh signaling acts in a paracrine fashion from tumor cells to stromal cells because SMO inhibition in the mouse stroma of xenograft tumor models is required for growth inhibition.¹⁵ While this explains the lack of GLI modulation in human tumor cells by **5** in our HT29 xenograft study, at the time we also wanted to rule out potential inter-species potency differences between mouse and human SMO as the cause. Our primary assay for potency optimization utilized a mouse cell line(C3H10T1/2) and aligning human and mouse SMO sequences revealed 92% similarity which raised our concern regarding inter-species binding affinity difference. Seeking to understand the risk that we might have inadvertently optimized **5** for mouse SMO inhibition over its human isoform, we developed a competition binding assay (Bodipy-labeled cyclopamine) to test the affinity difference of **5** to mouse and human SMO, using **1** as the control. Interestingly, we observed similar binding potency for **1** in Hela cells transfected with either mouse or human SMO, whereas **5** showed a 7-fold decrease in affinity from mouse to human (**Figure 2**). Furthermore, when **1** and **5** were tested in a luciferase assay using Homo sapiens palatal mesenchyme cells (HEPM), we also observed notable IC50 value differences between these two compounds (0.4 nM vs. 2.4 nM for **1** and **5**, respectively). These two showed less difference in potency in our primary cellular assay using the mouse cell line C3H10T1/2 (4.7 nM for **1** vs. 12 nM for **5**, **Table 1**). This unexpected potency drop-off for **5** led us to deprioritize further preclinical studies on **5** and initiated additional exploration work for more potent SMO inhibitors. We continued to use the C3H10T1/2 differentiation assay as our primary assay and used the low throughput human SMO binding and HEPM assays to check key compounds to prevent unexpected species-dependent potency difference.

A:



B:



C:

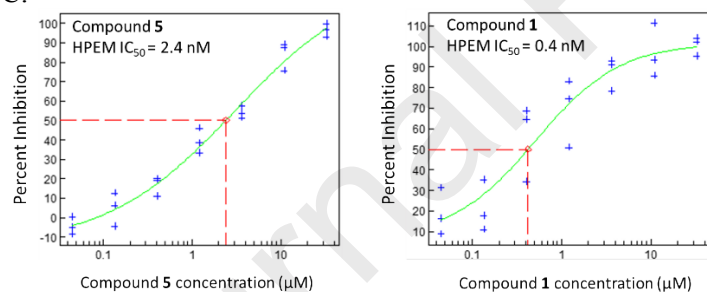
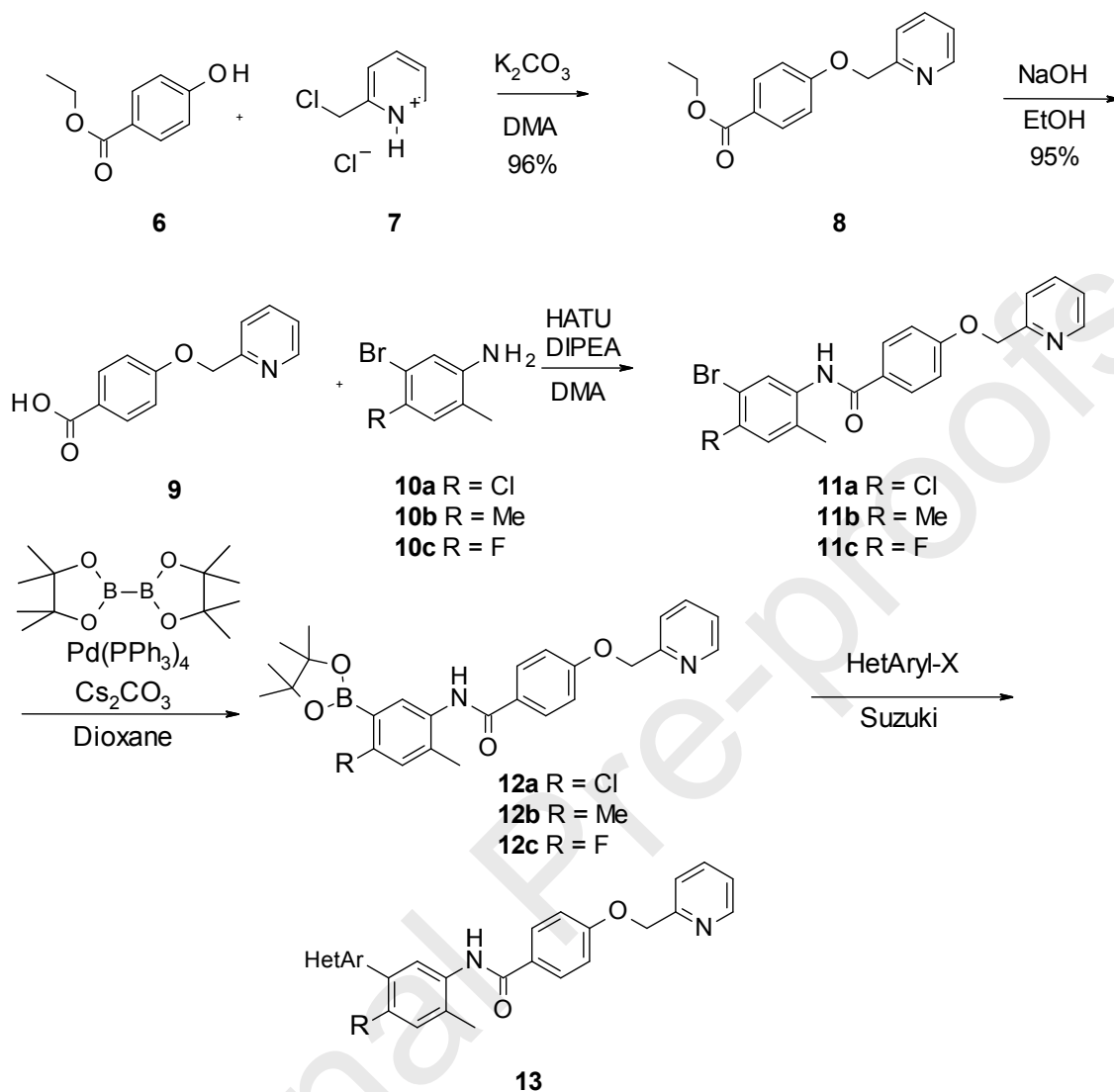


Figure 2. A: Binding EC_{50} of **1** in human and mouse SMO transfected Hela cells; B: Binding EC_{50} of **5** in human and mouse SMO transfected Hela cells; C: **5** and **1** induced luciferase inhibition in HPEM cells.

Synthesis of *ortho* substituted heteroarylamides.

The general synthetic route to a series of *ortho* substituted heteroarylamides is illustrated in **Scheme 1**.

The phenol in benzoyl ester **6** undergoes direct alkylation by reaction with chloromethylpyridine **7** in the presence of potassium carbonate. Hydrolysis of the corresponding ester product **8** under basic conditions results in carboxylic acid **9**. Amide coupling between the acid **9** and the trisubstituted anilines **10** using HATU as the coupling reagent and DIPEA as the base affords the bromoamide compounds **11**. The bromide can be converted to pinacol boronates **12** under Suzuki reaction conditions, and here we used palladium tetrakis as the catalyst and cesium carbonate as the base in anhydrous 1,4-dioxane. The resulting arylboronates **12** were further coupled with heteroaryl halide, again using Suzuki coupling conditions particularly with 1'-bis(di-tert-butylphosphino)ferrocene]-dichloropalladium (II) (Pd(dt-bpf)Cl₂) as the catalyst, to generate a series of heteroaryl substituted benzamide compounds (**13**).



Scheme 1. Synthetic route to heteroaryl substituted benzamides (heteroarylamides).

4-Cl on aniline core and *o*-Me on imidazoles for torsional twist.

Suspecting that the chloro group *ortho* to the pyridyl in **1** increased the torsional twist between the aniline phenyl and the pyridyl ring, we envisioned that tuning the dihedral angle between the heteroaryl group and the aniline phenyl in our heteroarylamide series could also benefit the potency, with the assumption that the heteroarylamides bind to the same pocket and with a similar pose in SMO as **1**. We then employed Quantum-Mechanics (QM) to perform a torsion scan of **1** (Supporting

Information, **Figure S3**), which indeed revealed two minima at 140° and 240° (**Figure 3A**).

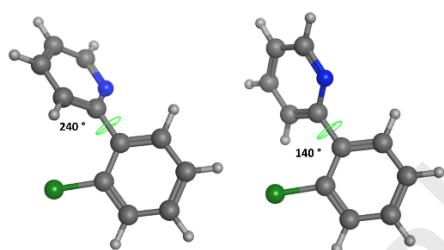
We therefore sought to design and investigate heteroarylamides which showed similar torsional preferences as **1**, anticipating that one of these two dihedral twists may be representative of the bioactive conformation. Although we lacked structural understanding of how the twisted conformation might increase the potency of compounds **1** or analogues of **5** at the time, we reasoned the twisted heteroaryl rings might allow for favourable π - π interactions with the protein, allow the nitrogen electron lone pairs of the heteroaryls to form polar interactions with the protein, or might simply offer improved receptor-ligand complementarity in the ground state conformation of the ligand.

We first synthesized three imidazole benzamides with the requisite 4-Cl on the aniline ring, and compared their potency in a cell based shh stimulated C3H10T1/2 differentiation assay to the 4-H analogues that were previously disclosed.¹⁶ We were gratified to observe consistent improvements in potency upon introduction of the 4-Cl group, notably in the case of 1,2-dimethylimidazole compounds (**17** and **18**), a ~10-fold improvement was achieved. While the gain in potency was encouraging, we were intrigued by the likely contributing factors to the observed potency difference between these 4-Cl and 4-H matched pairs. The introduction of the 4-Cl group resulted in notably higher measured LogD vs. their 4-H matched pairs, demonstrated by two 1-methylimidazole compounds (**15** vs. **16**) and two 1,2-dimethyl imidazole compounds (**17** vs. **18**), suggesting that the potency improvement was likely due to increased lipophilicity rather than a conformational change. The increased LogD with 4-Cl substitution was also accompanied by decreased solubility (**Table 1**, **14** and **18** aqueous solubility < 1 μ M).

Without observing significant potency improvement independent of the lipophilicity, we next performed a QM based torsion scan between the aniline and imidazole rings of the compounds in

Table 1. Interestingly, a planar torsion was predicted to be adopted by the 4-Cl imidazole compound (**14**), like the 4-H imidazole **5** (**Figure 3B**). We suspected an intramolecular hydrogen-bond locked the Cl and the H-bond donor NH from the imidazole group.¹⁷ Similar behaviour was seen in the other matched pairs **15** vs. **16** and **17** vs. **18**, and in both matched pairs an internal hydrogen-bond likely formed between the CH of the imidazole and the Cl atom. The free energy difference between the favoured torsional angle and the perceived 140°/240° bioactive torsion was not seen to change significantly for Cl-containing species compared to their H-containing matched pairs, supporting the hypothesis that the increase in potency was predominantly driven by LogD. We characterised the free energy difference as ΔE_{bio} , calculated as the average energy required to adopt either the 140°/240° bioactive dihedral relative to the lowest energy torsion.

A:



B:

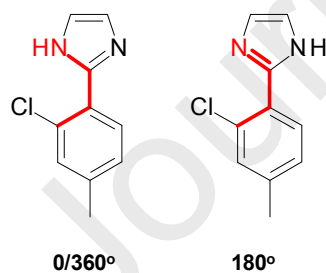
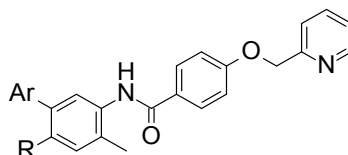


Figure 3. A: Depiction of the minima dihedral angles between the pyridyl and *o*-Cl-phenyl from QM based torsion scan; B: Illustration of 0° and 180° dihedral angles between the imidazole and phenyl rings when two aromatic rings adopt co-planar conformation.

Table 1. 4-Cl substituted heterobiaryl amides increased potency but at the expense of LogD.

Compound	Ar	R	shh EC ₅₀ (nM) ^a	LogD	Solubility (μM) ^b	φ ^c	ΔE _{bio} (kcal/mol)
1			4.7	2.8	6	140°	
5		H	13	3.0	25	190	2.5
14		Cl	7.5	>3.0	<1	350	2.6
15		H	89	2.5	80	180	2.6
16		Cl	23	3.1	20	0	2.5
17		H	27	2.7	46	180	2.6
18		Cl	2.9	3.3	<1	10	2.3

^a C3H10T1/2 differentiation stimulated by sonic Hh protein (shh) was previously described.¹⁶ EC₅₀ values are the geometric mean of at least two tests.

^b Solids from evaporated DMSO solutions were used to measure solubility.

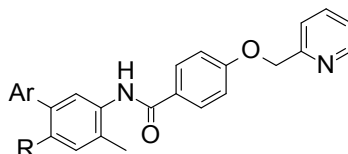
^c Calculated torsional angles between the heteroaryl ring and the phenyl ring using the Becke3LYP functional¹⁸ and the 6-311+G* basis set.

Given that the 4-Cl substitution did not appear to favour a notable torsional twist between the two aromatic rings, together with the unwanted LogD increase and deterioration in solubility, we revisited the impact on the torsion angle by the *o*-Me groups on the 5-membered imidazole rings that we previously synthesized (**Table 2**). Matched pair analysis showed that *o*-Me substituted imidazoles all resulted in a reduced ΔE_{bio} compared to *o*-H, indicating a lower barrier to twisting the biaryl away from coplanarity. However, it is noteworthy the *o*-Me substitution on the imidazole nitrogen (**19** and

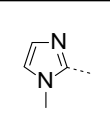
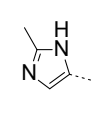
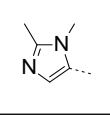
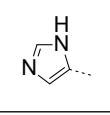
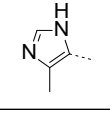
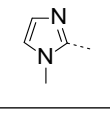
21) reduced the potency relative to their NH matched pairs, **5** and **20**, respectively. In contrast, the *o*-Me substitution on a carbon atom of the imidazole, while retaining the NH group, showed similar potency (**22** vs. **23**). The subtle SAR led us to suspect that the NH group, likely as a H-bond donor, might make a favorable polar interaction in the binding pocket of SMO. As a result, although the reduced energy barrier (ΔE_{bio}) to adopt the perceived bioactive twisted conformation by *o*-Me substitutions might favor the SMO-ligand interaction, the elimination of a possible polar interaction between the imidazole NH and SMO protein compromised the benefit to potency from *o*-Me substitution.

Compound **24** is a matched pair to both **14** (4-Cl substitution on the aniline core) and **19** (N-Me substitution on the imidazole group). The N-Me substitution neutralized the favourable torsion twist induced by the 4-Cl substitution, resulting in **24** but with no potency gain from **14**. The slight improvement in potency for **24** over **19** was consistent with a reduced ΔE_{bio} and the increase of LogD (+ 0.4). Compound **24** also showed a reduction in solubility relative to **19**, retaining the trend we observed in compounds shown in **Table 1**. We consistently observed that the methyl substituents on these imidazoles generally maintain or slightly reduce LogD, presumably through their electron donating effect to increase the pK_a of the imidazole nitrogen. However, a more notable effect of these methyl groups on physical properties is that they sometimes strongly increased the solubility of this series of compounds, in marked contrast to the 4-Cl substitution on the middle aniline ring.

Table 2: *o*-Me substitution on imidazole improves physical properties



Compound	Ar	R	shh EC ₅₀ (nM) ^a	LogD	Solubility (μM)	ϕ	ΔE_{bio} (kcal/mol)
----------	----	---	---	------	---------------------------------	--------	---------------------------------------

19		H	18	2.8	192	210	1.1
20		H	6.7	3.0	15	160	1.7
21		H	30	2.8	371	140	0.5
22		H	39	2.8	90	160	1.6
23		H	21	2.9	123	160	0.6
24		Cl	6.8	3.2	1	300	0.2

^a EC₅₀ values are the geometric mean of at least two tests.

4-Me on aniline core to introduce torsional twist on heteroarylamides.

Having observed the potency gain with 4-Cl substitution on the middle aniline group and the beneficial physical property improvement with methyl substitution on the imidazole groups we then synthesized 4-Me analogues on the middle aniline, hypothesizing the 4-Me could improve the potency while retaining the promising physical properties. Intrigued by the subtle potency changes when 4-Cl was installed, we also looked for additional *ortho* substitution groups, such as 4-F. Here we observed remarkable improvement in potency in the shh induced cell differentiation assay, particularly for **25** (EC₅₀ 1.4 nM) where the 4-Me substitution showed a near 10-fold increase over **5** (EC₅₀ 13 nM).

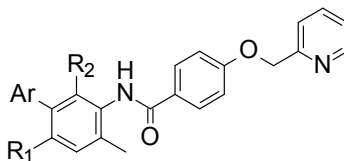
Compound **25** has both a lower ΔE_{bio} and a more orthogonal ground state conformation (210°) relative to **5**, indicating that it can adopt the presumed bioactive conformation more readily (**Table 3**). The substitution of Cl and Me on phenyl groups is normally considered to be bioisosteric due to their

similar size,¹⁹ yet here we observed remarkable potency differences between these two substituents. The QM torsional analysis revealed that Cl-containing analogues can form an intramolecular H-bond to either the *ortho* NH or CH on the linking heterocycle, whilst the Me-containing compounds cannot. This results in a reduced energy barrier to adopt the perceived binding mode for the Me-containing compounds which is consistent with their boost in potency relative to Cl-analogues.

The potency gain in **26** (EC_{50} 2.6 nM) is even more noteworthy at 34-fold compared to its 4-H analogue **15** (EC_{50} 89 nM). Both **25** and **26** are also more potent than their 4-Cl analogues (**14** and **16**), consistent with a reduction in ΔE_{bio} . Furthermore, they also showed a smaller LogD increase compared to the chloride analogues. Similar to the 4-Cl compounds, both **25** and **26** still showed a trend for decreased solubility. We also tested **25** and **26** in rat and human hepatocyte stability assays, and while both compounds showed moderate Cl_{int} values, there was an overall increase relative to their 4-H matched pairs. The 4-Me substitution in **27** also showed 10-fold improvement in potency over the 4-H compound **21**, but it came with some decreased metabolic stability (rat hepatocytes Cl_{int} 32 μ l/min/ 10^{-6} cells and human hepatocytes Cl_{int} 12 μ l/min/ 10^{-6} cells) and hERG inhibition liability also increased (IC_{50} 12 μ M).

The 4-F compound **28** showed no improvement of potency over its 4-H analogue **5**, consistent with no improvement of ΔE_{bio} . A clear disadvantage of 4-F substitution as shown in **28** is its notably reduced solubility. Anticipating the 2-Me substitution (R2) could induce a similar dihedral twist as 4-Me on the aniline ring, we also synthesized **29**. However, compound **29** showed no potency gain over **5**, potentially owing to conformational effects on the adjacent amide moiety.

Table 3. 4-Me and 4-F substituted heteroaryl amides.



	Ar	R ₁	R ₂	shh EC ₅₀ (nM) ^b	LogD	Solubility (μM) ^c	Heps Clint (ul/min/10 ⁻⁶)		hERG IC ₅₀ (μM)	φ ^a	ΔE _{bio} (kcal/ mol)
							Rat	Human			
25		Me	H	1.0	3.1	2	18	9	>28	210	1.5
26		Me	H	2.6	3.0	8	19	6	21	170	0.8
27		Me	H	2.9	2.8	ND ^d	32	12	12	220	0.1
28		F	H	17	3.0	1	14	ND ^d	>100	0	4.5
29		H	Me	13	2.8	69	ND ^d	ND ^d	>100	150	1.9

^a Calculated torsional angles between the heteroaryl ring and the phenyl ring using the Becke3LYP functional and the 6-311+G* basis set.

^b EC₅₀ values are the geometric mean of at least two tests.

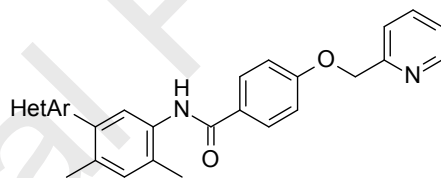
^c Solids from evaporated DMSO solutions were used to measure solubility.

^d Not determined.

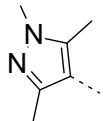
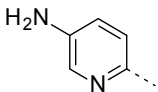
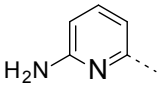
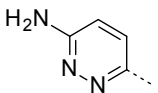
Encouraged by the significant potency gain from the 4-Me substitution, we next synthesized a small set of 4-Me heteroaryl amides, structurally diversifying from the imidazoles into other heteroaryls, including pyrazole, thiazole, pyridyl, and pyridazine (**Table 4**). The potency difference among these compounds is relatively insignificant, but it could also be that the measured potency was reaching the limit of the test concentration range of our cellular assay. For most of these compounds, one concern was the increased lipophilicity in comparison with the imidazole amides, as some of them failed to give numerical readouts in LogD measurement, possibly due to their poor solubility and high lipophilicity (e.g. the benzimidazole analogue **30** and 3-pyridyl analogue **35**). The thiazole compound

31 showed excellent potency, but its HLM (human liver microsome) and RLM (rat liver microsome) Cl_{int} were too high to be acceptable. Two pyrazole analogues, **32** and **33**, exhibited similar potency and improved solubility, with **32** showing better metabolic stability in both rat and human liver microsomes. 2-Pyridyl compound **34** and 3-pyridyl compound **35** showed subtle differences in potency (0.8 vs. 2.3 nM) that may imply the 2-pyridyl nitrogen is making polar interaction with the SMO protein while 3-pyridyl N is not as optimally positioned to make the same interaction. However, neither compound was chosen for further studies due to their higher metabolic Cl_{int} s. Surprisingly, the two aminopyridine analogues **36** and **37** showed little difference in potency despite the different orientation of their amino groups. Although the amino group presumably affords additional hydrophilicity, both **36** and **37** failed to show meaningful improvement in solubility. The aminopyridazine compound **38** was of interest as it brought together excellent potency and metabolic stability in both human and rat liver microsomes, although solubility continued to be a concern.

Table 4. Non-imidazole heterobiaryl amides with 4-Me substitution



Compound Name	HetAr	shh EC_{50} (nM) ^a	LogD	Solubility (μ M)	RLM Cl_{int} (μ l/min/mg)	HLM Cl_{int} (μ l/min/mg)
30		3.1	>3.5	<1	21	30
31		0.9	>3.0	<1	147	513
32		1.1	>3.0	33	55	20

33		3.1	>3.0	35	271	122
34		0.8	>3.0	<1	296	209
35		2.3	>3.0	9	78	62
36		1	3.2	<1	32	9
37		1.7	>3.0	2	155	88
38		<1.5	2.6	6	8	<4

Binding mode of heterobiaryl amides to SMO

As transmembrane proteins, GPCRs were notoriously difficult to crystallize and as a result the binding modes of GPCR inhibitors, including SMO inhibitors, largely remained mysterious for decades.

However, recent advancements in protein crystallography have begun to unveil the complex signal transduction mechanism of the Hh pathway, where SMO plays a key regulatory role.¹²⁻¹³ The co-crystallization of cyclopamine and vismodegib with SMO offered insight into the transmembrane binding pocket of SMO.¹⁰⁻¹¹ It is interesting to note this binding pocket is close to the extracellular domain CRD and is likely accessible to SMO ligands without the need for them to first enter the cell.

With the recently available X-ray structure of SMO, we retrospectively docked our heteroarylamides into the SMO transmembrane pocket that vismodegib occupies (PDB 5L7I),¹² and illustrated in

Figure 4 is the predicted binding mode of **25**. As anticipated, the imidazole and the aniline rings are predicted to adopt a significant twisted conformation of 228°, close to the dihedral angle adopted by vismodegib in SMO (240°). This twisted conformation between the two aromatic rings in **25** allows

some key ligand-protein interactions: 1) the imidazole group forms edge-to-plane π - π interactions, one with the indole group of Trp281 and another with His470, explaining the improved potency when the dihedral twist is induced by 4-Me substitution; and 2) the hydrogen bond between the imidazole NH and the phenol group of Tyr394. Interestingly, in addition to forcing the bioactive dihedral twist, 4-Me also makes favourable hydrophobic contacts with some lipophilic residues in the binding pocket, notably the isobutyl and the methyl sulfide sidechains of Leu522 and Met230. The core amide group of this series of compounds also makes two key interactions, forming hydrogen bonds with the guanidine group of Arg400 and the acid group of Asp384.

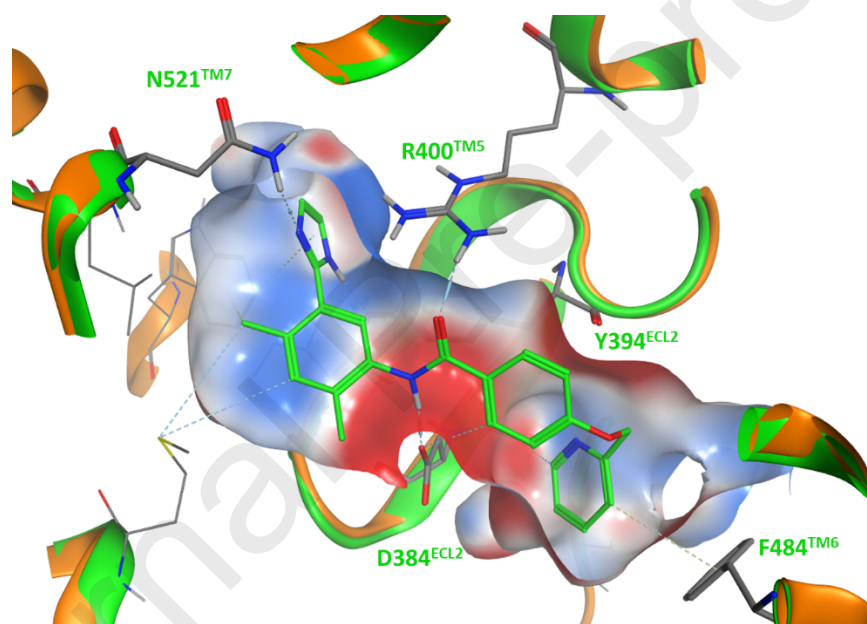


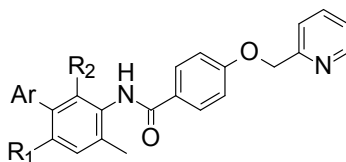
Figure 4. Predicted binding mode of **25** in SMO (**25** and SMO ribbon are in green and key residue side chains are in grey). Key polar interactions between the ligand and the protein residues were shown as dotted lines. Key interacting residue were labelled.

In vivo studies with SMO inhibitors

For pharmacological evaluation, we chose Colo205 mouse xenografts as the in vivo model for pharmacodynamics (PD) screening to measure the expression of murine Hh pathway genes and the decrease in murine GLI (mGLI) after treatment with SMO inhibitors. Female nude mice were

implanted with 5M Colo205 cells subcutaneously. Once tumors reached >200 mm³ in size, animals were treated with a single oral dose of the treatment compound. At 1 and 8 h, mice were sacrificed, and tumors were analyzed for mGLI levels by RT-PCR and blood plasma samples were assessed for drug concentrations. Maximal inhibition of mGLI achieved in this model was observed at 6 and 8 hours post dose (Supporting Information, **Figure S1**). Summarized in **Table 5** are the PK/PD results for some of the SMO inhibitors **25**, **26**, **32**, **38**, and a few of their structurally matched pairs, as well as the key tool compounds **1** and **5**. For each compound, mGLI inhibition was measured after 8 hours of the single dose (40 mg/kg) and normalized vs. the vehicle control group; Mouse plasma PK was measured at two timepoints, 1 hour and 8 hours. Shown in **Table 5** is also the human and mouse plasma protein binding (PBB) free fraction to allow estimation of free concentration of compound in mouse.

Compound **1** demonstrated excellent oral exposure in mouse and significantly decreased mGLI mRNA expression (82%). Four compounds featuring imidazole groups (**5**, **25**, **26**, and **29**) showed different oral exposure levels as shown by plasma concentrations, with compound **5** and its 4-F analogue **28** achieving significantly higher plasma concentration than the 4-Me analogue **25**, but nevertheless **25** showed the highest mGLI inhibition (88%). The decreased potency coupled with poor plasma exposure of **29** resulted in no observable mGLI inhibition. Consistent with the potency gain in the shh C3H10T1/2 differentiation assay for 4-Me analogues, two matched pairs, **15** vs. **26** and **22** vs. **27**, showed notable difference in mGLI inhibition despite the similar plasma concentrations between each matched pair. This further underlined the significance of 4-Me substitution in enhancing the potency of this series of heteroaryl amide compounds. The pyrazole compound **32**, however, showed relatively poor exposure in mouse and as a result less inhibition of mGLI (75%). The pyridazine compound **38**, despite its higher concentration than **25**, produced slightly less mGLI inhibition. The human PBB free fractions of these compounds are generally similar, except the noticeably lower free fraction for **1**.

Table 5. Mouse GLI mRNA inhibition in a Colo205 xenograft PD model

Compound Name	R ₁	R ₂	Hu / mouse PPB (% free)	Plasma Concentration (1 h) (μ M)	Plasma Concentration (8 h) (μ M)	% inhibition mGLI (8 h)
1			<1.0 ^a / 2.6	10.3	18.8	82%
5	H	H	6.0 / 4.0		7.5	79%
25	Me		7.1 / 3.3	22.3	1.9	88%
28	F		11 / -	58	20	73%
29	H	Me	9 / -	3.3	0.14	0%
15	H	H	9.5 / -	63	16	39%
26	Me		5.5 / 1.2	94	16	87%
21	H	H	19 / -	1.8	0.08	12%
27	Me		9.5 / -	2.9	0.28	81%
32	Me	H	2.1 / -	5.5	0.23	75%
38	Me	H	6.4 / 2.9	33	2.7	80%

^a Compound **1** was reported to have species-dependent PPB due to its strong binding to human α -1-acid glycoprotein (AAG).²⁰

Based on their attractive *in vivo* activity, we prioritized compounds **25** and **26** for more extensive preclinical evaluation. Both **25** and **26** were further tested in an HT29-MEF (murine embryonic fibroblast) co-implant xenograft model for anti-tumour efficacy. The HT29 model was set up with a suboptimal number of tumor cells (0.3 M) which were co-implanted with 1.5M MEF (GSC-6002, Globalstem, Rockville, MD) in nude mice to model the Hh/SMO paracrine signaling pathway. Treatment started when the average tumor volume reached approximately 85 mm³. Compounds **25** and **26** were dosed orally at 40 mg/kg twice daily for 10 days. As a result, both **25** and **26** exhibited 42% and 43% tumor growth inhibition respectively at $p < 0.01$ (**Figure 4**).

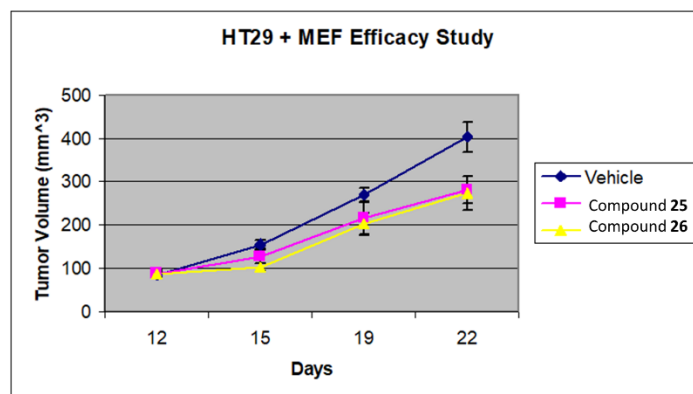


Figure 4. **25** and **26** in HT-29+MEF xenograft model showing tumor growth inhibition as single agents.

Human SMO potency and ADME properties of **25** and **26**

Because the Colo205 xenograft model measured the inhibition of mGLI mRNA expression, and we were conscious of the potential difference between mouse and human activity, we tested the respective binding affinity of **25** and **26** to mouse and human SMO (**Table 6**). Both compounds showed negligible difference in binding between these two species and demonstrated similar potency to **1** in human cell lines (HEPM) in inhibiting the Hh pathway, in line with their excellent binding affinity to human SMO. The potencies of **1** in these assays are also included in **Table 6**, illustrating that **26** possesses similar potency across these assays to **1**, but **25** shows better potency across these cell-based assays. The solubility of both **25** and **26** are low, but they were both able to be dosed as high as 100 mg/kg in rodents and still achieve dose proportional oral exposure (data not shown), indicating that their low aqueous solubility did not limit their oral absorption, likely due to their excellent permeability. We investigated their efflux potential and permeability using a human cell line engineered to express the P-gp efflux pump (MDR1-LLC PK1 cells), and the efflux ratios are 5.3 and 2 for **25** and **26**, respectively. The low efflux ratios indicate **25** and **26** as P-gp substrates, but the efflux ratios are relatively low, and the permeability of both compounds as assessed by A>B drug migration is deemed to be high (Papp A>B 7.5×10^{-6} cm/s and 16.5×10^{-6} cm/s for **25** and **26**,

respectively).

Table 6. Summary of preclinical data of **1**, **25**, and **26**

	1	25	26
Mouse shh IC ₅₀ (nM)	4.7	1	2.6
Binding EC ₅₀ (nM) human/mouse	2.0 / 3.0	0.5 / 20	1.5 / 3.1
HPEM IC ₅₀ (nM)	0.4	0.08	0.2
mGLI inhibition (40 mg/kg)	82%	88%	87%
LogD	2.8	3.1	3
Aqueous solubility pH7.4 (μM)	6	2	8
PPB (% free) mouse/rat/dog/human	2.6 / < 1.0 / - / < 1.0	3.3 / 6.0 / 11 / 6.7	1.2 / 1.0 / 7.2 / 5.5
Heps Clint (μl/min/1E6) mouse/rat/dog/human	- / 16 / - / < 1	6.6 / 18 / 1.4 / 9	< 1 / 19 / 10 / 6
Clearance (ml/min/kg) mouse/rat/dog/Guinea pig	5.6 / 2 / - / -	31 / 24 / 4.0 / 18	6.1 / 1.7 / 4.7 / 1.6
Vdss (L/kg) mouse/rat/dog/guinea pig	0.5 / 0.3 / - / -	1.6 / 1.2 / 0.9 / 1.8	0.4 / 0.2 / 0.5 / 0.5
t _{1/2} (h) mouse/rat/dog/guinea pig	1.0 / 1.9 / - / -	0.7 / 1.1 / 3.3 / 1.5	0.8 / 2.4 / 1.4 / 4.2
% Oral bioavailability mouse/rat/dog	33 / 49 / - / -	75 / 100 / 100	70 / 90 / 32
CYP 3A4, 2D6, 2C9, 2C19, 1A2 IC ₅₀ (μM)	all > 20	all > 20	2C9: 4.5
hERG IC ₅₀ (μM)	>33	25	23
MDR1-LLC PK1 (A > B) Papp (10 ⁻⁶ cm/s) / Efflux ratio	- / -	7.5 / 5.3	16.5 / 2

Compounds **25** and **26** have slightly different PK profiles in rodents. **25** shows moderate plasma clearance in both mouse and rat, while **26** more resembles the rodent PK profile of **1**, with remarkably low plasma clearance. However, even though **25** showed higher clearance in both mouse and rat, its plasma half-life (t_{1/2}) is similar to **26** and **1**, due to its higher volume of distribution. Given their similar physical properties and close structural resemblance, the difference in volume distribution between **25** and **26** in mouse and rat can be explained by their different free fraction in PPB in these two species, as **25** with higher free fraction in plasma produces a proportionally larger volume. Likewise, the smaller difference in dog PPB between these two compounds also correlates to their similar volumes in dog. Judging by their comparable human protein binding free fraction, it is

reasonable to expect the human volume of these two compounds will be similar, and considering their small differences in human hepatocyte Cl_{int} , we can expect their human plasma half-lives are likely to be in a similar range. In our hands both **25** and **26** demonstrated excellent oral bioavailability across mice, rats, and dogs. The bioavailabilities of **1** in mice and rats were limited by its absorption because **1** demonstrated very low clearance in both species.⁸ We also evaluated the drug-drug interaction potential of these compounds, and none of these three compounds showed cytochrome P450 inhibition liability. Lastly, both **25** and **26** were evaluated in a panel of cardiac ion channel assays; both compounds were shown to be inactive in Na^+ or K^+ ion channel assays but showed moderate hERG inhibition. Given their excellent cellular potency and predicted low efficacious concentrations in the clinic, the hERG activity did not prevent us from further preclinical safety studies. Both **25** and **26** were subsequently nominated for further pre-clinical studies as candidate drugs (AZD7254 and AZD8452,¹⁶ respectively).

Summary

In summary, our previous lead SMO inhibitor **5** showed an unexpected inter-species difference in its binding affinity towards SMO between mouse and human. In the absence of protein structural information, we methodically explored the SAR of this series of heteroarylamides and eventually identified a subseries of SMO inhibitors with improved potency and *in vivo* activity in mGLI expression inhibition. The 4-Me on the central aniline ring being *ortho* to the heteroaryl is critical for the improved potency, and the potency gained from the methyl group was explained both by introducing a twisted conformation between the two aromatic rings and its interaction with hydrophobic residues in the SMO transmembrane binding site. These dual effects of the 4-Me group in this subseries serves an example of the often sought-after “magic methyl” effect.²¹ Optimal heteroaryl groups were also found to make polar interactions with the binding pocket residues via hydrogen bonding interactions. Among these subseries of potent SMO inhibitors, compounds **25** and **26** were selected for their excellent *in vivo* activity in a Colo205 mouse xenograft model and both

compounds demonstrated good oral PK in multiple preclinical species and were predicted to have acceptable human PK to allow once daily dosing. On the basis of the above overall assessment, both **25** and **26** advanced into preclinical safety studies. Compound **26** (AZD8452) was discontinued due to potential cardiovascular risk found in GLP safety studies. Compound **25** (AZD7254) was late discontinued due to shifted business priorities.

EXPERIMENTAL

General information

All solvents used were commercially available in anhydrous grade. Reagents were utilized without further purification unless otherwise stated. Evaporation of solvent was carried out using a rotary evaporator under reduced pressure at a bath temperature of up to 60 °C. Temperatures are given in degrees Celsius (°C), and operations were carried out at room or ambient temperature, that is at a temperature in the range of 18-30 °C. In general, the course of reactions was followed by thin layer chromatography or mass spectroscopy and reaction times are given for illustration only; where a synthesis is described as being analogous to that described in a previous example, the amounts used are the millimolar ratio equivalents to those used in the previous example. NMR data is in the form of delta values for major diagnostic protons, given in parts per million (ppm) relative to tetramethylsilane(TMS) as an internal standard, determined at 300 MHz or 400 MHz using deuterated solvent. Analytical mass spectra were run with an electron energy of 70 eV in the chemical ionization (CI) mode using a direct exposure probe; where indicated ionization was effected by electron impact (EI), electrospray (ESP), or atmospheric pressure chemical ionization (APCI); values for m/z are given; generally, only ions which indicate the parent mass are reported. Unless otherwise indicated, all final compounds were purified to $\geq 95\%$ purity, as assessed by analytical HPLC using an Agilent 1100 equipped with Waters columns (Atlantis T3, 2.1×50 mm, $3 \mu\text{m}$ or Atlantis C18, 2.1×50 mm, $5 \mu\text{m}$) eluted for >10 min with a gradient mixture of water and acetonitrile with either formic acid or ammonium acetate added as a modifier, monitored at wavelengths of 220, 254, and 280 nm. All

experimental activities involving animals were carried out in accordance with AstraZeneca animal welfare protocols, which are consistent with The American Chemical Society Publications rules and ethical guidelines.

5-bromo-4-chloro-2-methylaniline (10a)

In a 200-mL round-bottomed flask was placed 1-bromo-2-chloro-4-methyl-5-nitrobenzene (4 g, 16 mmol) and FeCl₃ in silica gel (5%, 11.2 g) in MeOH (50 mL). The reaction mixture was heated to 70 °C for 15 min and then hydrazine monohydrate (8.8 mL, 192 mmol) was slowly added and the reaction mixture was refluxed overnight. After cooled to RT, the mixture was filtered, and concentrated in vacuo to afford the title compound (3.4 g) in 95% yield. ¹H NMR (DMSO-d₆) δ 1.98 (s, 3 H), 6.90 (s, 1 H), 7.10 (s, 1 H).

N-(5-bromo-4-chloro-2-methylphenyl)-4-(pyridin-2-ylmethoxy)benzamide (11a). In a 100-mL round-bottomed flask was dissolved 4-(pyridin-2-ylmethoxy)benzoic acid (800 mg, 4 mmol) in SOCl₂ (6 mL). The solution was stirred for 1 h at RT. The solution was concentrated in vacuo to give 4-(pyridin-2-ylmethoxy)benzoyl chloride. The crude product was dissolved in DCM (10 mL) followed by the addition of 5-bromo-4-chloro-2-methylaniline (500 mg, 2.27 mmol), pyridine (5 mL), and TEA (10 mL). The reaction mixture was heated to 50 °C and stirred for 2h. The mixture was concentrated in vacuo and the crude product was purified by ISCO MPLC (20-33% EtOAc/petroleum ether) to afford the title compound (270 mg) in 28% yield. ¹H NMR (DMSO-d₆) δ 2.05 (s, 3 H), 2.25 (s, 2 H), 7.13 (m, 2 H), 7.34 (m, 1 H), 7.54 (m, 2 H), 7.77 (s, 1 H), 7.84 (m, 1 H), 7.92 (m, 2 H), 8.58 (m, 1 H), 9.81 (s, 1 H).

N-(4-chloro-2-methyl-5-(4,4,5,5-tetramethyl-1,3,2-dioxaborolan-2-yl)phenyl)-4-(pyridin-2-ylmethoxy)benzamide (12a). In a 10 mL vial was added 4,4,4',4',5,5,5',5'-octamethyl-2,2'-bi(1,3,2-dioxaborolane) (0.441 g, 1.74 mmol), N-(5-bromo-4-chloro-2-methylphenyl)-4-(pyridin-2-ylmethoxy)benzamide (0.5 g, 1.16 mmol), and KOAc (0.341 g, 3.47 mmol) in dioxane (80 mL) to give a

colorless suspension. Nitrogen was bubbled in for 20 min before Pd(PPh₃)₄ (0.134 g, 0.12 mmol) was added. The reaction was stirred at 115 °C in a microwave for 5h. After concentration under reduced pressure, the crude product was purified by ISCO MPLC (0-5% MeOH in DCM) to give the title compound. ¹H NMR (DMSO-d₆) δ 1.07 (s, 6 H), 1.16 (s, 6 H), 2.22 (s, 3 H), 5.28 (s, 2 H), 7.16 (d, 2 H), 7.36 (s, 1 H), 7.54 (d, 1 H), 7.59 (s, 1 H), 7.63 (m, 1 H), 7.85 (m, 1 H), 7.96 (m, 2 H), 8.60 (d, 1 H), 9.82 (s, 1 H).

N-[4-chloro-5-(1H-imidazol-2-yl)-2-methylphenyl]-4-(pyridin-2-ylmethoxy)benzamide (14). In a 10 mL vial was added N-(4-chloro-2-methyl-5-(4,4,5,5-tetramethyl-1,3,2-dioxaborolan-2-yl)phenyl)-4-(pyridin-2-ylmethoxy)benzamide (0.15 g, 0.31 mmol), 2-bromo-1H-imidazole (0.070 g, 0.5 mmol), and KOAc (0.077 g, 0.78 mmol) in dioxane (3.0 mL) to give a brown suspension. The reaction mixture was diluted with water (1.0 mL). Nitrogen was bubbled in for 20 min before Pd(PPh₃)₄ (0.036 g, 0.03 mmol) was added. The reaction was heated using a microwave at 130 °C for 2 h. After concentration *in vacuo*, the residue was diluted with MeOH (0.5 mL) and DMSO (0.5 mL). The solution was filtered and purified by Gilson HPLC (5-80% MeCN/0.1% TFA in water) to give the title compound as the product (0.012 g, 9% yield). ¹H NMR (DMSO-d₆) 2.37 (s, 3 H), 5.34 (s, 2 H), 7.20 (d, 2 H), 7.43 - 7.51 (m, 1 H), 7.63 (d, 1 H), 7.73 (s, 1 H), 7.86 - 7.91 (m, 3 H), 7.93 - 8.04 (m, 3 H), 8.66 (d, 1 H), 10.04 (s, 1 H), 14.85 (br s, 2 H); MS (M+H⁺) = 419.

Compounds **16**, **18**, and **20** were synthesized using the similar reaction as described in the synthesis of compound **14** from intermediate **12a**.

N-[4-chloro-2-methyl-5-(1-methyl-1H-imidazol-4-yl)phenyl]-4-(pyridin-2-ylmethoxy)benzamide (16). ¹H NMR (DMSO-d₆) 2.31 (s, 3 H), 3.92 (s, 3 H), 5.34 (s, 2 H), 7.19 (d, 2 H), 7.44 - 7.52 (m, 1 H), 7.60 - 7.68 (m, 2 H), 7.78 (s, 1 H), 7.94 - 8.04 (m, 3 H), 8.12 (s, 1 H), 8.66 (d, 1 H), 9.19 (s, 1 H), 9.98 (s,

1 H); MS (M+H⁺) = 433.

N-[4-chloro-5-(1,2-dimethyl-1H-imidazol-4-yl)-2-methylphenyl]-4-(pyridin-2-ylmethoxy)benzamide (18). ¹H NMR (DMSO-d₆) 2.30 (s, 3 H), 2.63 (s, 3 H), 3.80 (s, 3 H), 5.34 (s, 2 H), 7.19 (d, 2 H), 7.47 (m, 1 H), 7.63 (m, 2 H), 7.77 (s, 1 H), 7.97 (m, 3 H), 8.07 (s, 1 H), 8.65 (d, 1 H), 9.98 (s, 1 H); MS (M+H⁺) = 447.

N-[4-chloro-2-methyl-5-(1-methyl-1H-imidazol-2-yl)phenyl]-4-(pyridin-2-ylmethoxy)benzamide (20). ¹H NMR (DMSO-d₆) δ 2.38 (s, 3 H), 3.72 (s, 3 H), 5.33 (s, 2 H), 7.19 (d, 2 H), 7.46 (m, 1 H), 7.62 (d, 1 H), 7.76 (s, 1 H), 7.95 (m, 6 H), 8.65 (d, 1 H), 10.04 (s, 1 H). MS (M+H⁺) = 433.

N-(5-bromo-2,4-dimethyl-phenyl)-4-(2-pyridylmethoxy)benzamide (11b). In a round-bottomed flask was placed 5-bromo-2,4-dimethylaniline (5 g, 25 mmol), 4-(pyridin-2-ylmethoxy)benzoic acid (6.3 g, 26.5 mmol), and DIPEA (8.9 mL, 50 mmol) in DMF (50 mL). The mixture was cooled to 0 °C with a water-ice bath before HATU (11.5 g, 30 mmol) was added. The mixture was warmed to RT and stirred overnight. To the reaction solution was added water (200 mL). The precipitate was collected by filtration to afford the title compound (4 g, 41% yield). ¹H NMR (DMSO-d₆) δ 2.14 (s, 3 H), 2.27 (s, 3 H), 5.26 (s, 2 H), 7.13 (d, 2 H), 7.23 (s, 1 H), 7.34 (m, 1 H), 7.52 (t, 1 H), 7.56 (s, 1 H), 7.82 (m, 1 H), 7.92 (d, 2 H), 8.57 (m, 1 H).

N-(2,4-dimethyl-5-(4,4,5,5-tetramethyl-1,3,2-dioxaborolan-2-yl)phenyl)-4-(pyridin-2-ylmethoxy)benzamide (12b). In a round-bottomed flask was added N-(5-bromo-2,4-dimethylphenyl)-4-(pyridin-2-ylmethoxy)benzamide (4g, 9.73mmol), bis(pinacolato)diboron (2.96 g, 11.6mmol), and KOAc (2.86 g, 29.2 mmol) in dioxane (50 mL) to give a suspension. To the mixture was added PdCl₂(dppf) (400 mg). The reaction was stirred at 80 °C under a nitrogen atmosphere overnight. The reaction mixture was concentrated in vacuo and water (80 mL) was added. The mixture was extracted with EtOAc (2 X 30

mL) and the combined organic layers were dried (Na_2SO_4), then concentrated in vacuo to afford the crude product which was purified by ISCO MPLC (1% MeOH/DCM) to give the title compound (2.3 g, 52% yield). ^1H NMR (DMSO-d_6) δ 1.26 (s, 12 H), 2.15 (s, 3 H), 2.41 (s, 3 H), 5.25 (s, 2 H), 7.06 (s, 1 H), 7.12 (m, 2 H), 7.35 (m, 1 H), 7.51 (m, 2 H), 7.81 (m, 1 H), 7.94 (m, 2 H), 8.58 (m, 1 H), 9.71 (s, 1 H).

N-[5-(1H-imidazol-2-yl)-2,4-dimethylphenyl]-4-(pyridin-2-ylmethoxy)benzamide (25). In a 10 mL vial was added N-(2,4-dimethyl-5-(4,4,5,5-tetramethyl-1,3,2-dioxaborolan-2-yl)phenyl)-4-(pyridin-2-ylmethoxy)benzamide (0.25 g, 0.55 mmol), 2-bromo-1H-imidazole (0.12 g, 0.82 mmol), and Cs_2CO_3 (0.44 g, 1.36 mmol) in dioxane (5 mL) to give a brown suspension. The reaction mixture was diluted with water (2 mL). Nitrogen was bubbled in for 20 min before $\text{Pd}(\text{PPh}_3)_4$ (0.063 g, 0.05 mmol) was added. The reaction was heated at 110 °C for 4h under microwave conditions. The reaction mixture was concentrated under reduced pressure. The residue was purified by Gilson HPLC (MeCN/0.1% TFA in water). To the purified product was added HCl in Et_2O (0.5 mL, 1 mmol). The mixture was concentrated in vacuo to give the HCl salt of the title compound (10 mg, 4.2%). ^1H NMR (DMSO-d_6) δ 2.31 (s, 3 H), 2.36 (s, 3 H), 5.32 (s, 2 H), 7.18 (d, 2 H), 7.39 (s, 1 H), 7.45 (br s, 1 H), 7.61 (s, 2 H), 7.84 (s, 2 H), 7.96 (m, 3 H), 8.63 (d, 1 H), 9.90 (s, 1 H), 14.54 (br s, 1 H); MS ($\text{M}+\text{H}^+$) = 399.

Compounds below were synthesized following the general synthetic route as shown above for **25**.

N-[2,4-dimethyl-5-(1-methyl-1H-imidazol-4-yl)phenyl]-4-(pyridin-2-ylmethoxy)benzamide (26). ^1H NMR (DMSO-d_6) 2.26 (s, 3 H), 2.37 (s, 3 H), 3.92 (s, 3 H), 5.37 (s, 2 H), 7.18 (d, 2 H), 7.30 (s, 1 H), 7.53 (m, 2 H), 7.69 (d, 1 H), 7.91 (s, 1 H), 8.02 (m, 3 H), 8.69 (d, 1 H), 9.21 (s, 1 H), 9.87 (s, 1 H); MS ($\text{M}+\text{H}^+$) = 413.

N-[5-(1,2-dimethyl-1H-imidazol-5-yl)-2,4-dimethylphenyl]-4-(pyridin-2-ylmethoxy)benzamide (27).

¹H NMR (DMSO-d₆) 2.16 (s, 3 H), 2.28 (s, 3 H), 2.62 (m, 3 H), 3.46 (s, 3 H), 5.33 (s, 2 H), 7.17 (d, 2 H), 7.33 (d, 2 H), 7.47 (m, 1 H), 7.63 (m, 2 H), 7.97 (m, 3 H), 8.65 (d, 1 H), 9.83 (s, 1 H), 14.38 (br s, 1 H); MS (M+H⁺) = 427.

N-[5-(1H-benzimidazol-2-yl)-2,4-dimethylphenyl]-4-(pyridin-2-ylmethoxy)benzamide (30).

¹H NMR (DMSO-d₆) 2.35 (s, 3 H), 2.55 (s, 3 H), 5.37 (s, 2 H), 7.20 (d, 2 H), 7.46 (s, 1 H), 7.52 (m, 1 H), 7.60 (m, 2 H), 7.68 (d, 1 H), 7.83 (s, 1 H), 7.87 (m, 2 H), 8.01 (m, 3 H), 8.68 (d, 1 H), 9.99 (s, 1 H); MS (M+H⁺) = 449.

N-[2,4-dimethyl-5-(4-methyl-1,3-thiazol-2-yl)phenyl]-4-(pyridin-2-ylmethoxy)benzamide

(31). ¹H NMR (DMSO-d₆) 9.81 (br. s., 1 H), 8.68 (d, 1 H), 8.03 - 8.28 (m, 1 H), 7.94 (d, 2 H), 7.65 - 7.80 (m, 2 H), 7.50 - 7.65 (m, 1 H), 7.31 (s, 1 H), 7.19 (s, 1 H), 7.12 (d, 2 H), 5.36 (s, 2 H), 2.46 (br. s., 3 H), 2.37 (s, 3 H), 2.17 (s, 3 H); MS (M+H⁺) = 430.

N-[2,4-dimethyl-5-(3-methyl-1H-pyrazol-4-yl)phenyl]-4-(pyridin-2-ylmethoxy)benzamide (32).

¹H NMR (DMSO-d₆) 2.11 (s, 3 H), 2.16 (d, 6 H), 5.42 (s, 2 H), 7.02 - 7.18 (m, 5 H), 7.63 - 7.75 (m, 1 H), 7.83 (d, 1 H), 7.88 - 7.99 (m, 3 H), 8.22 (t, 1 H), 8.73 (d, 1 H), 9.72 (s, 1 H); MS (M+H⁺) = 413.

N-[2,4-dimethyl-5-(1,3,5-trimethyl-1H-pyrazol-4-yl)phenyl]-4-(pyridin-2-ylmethoxy)benzamide

(33). ¹H NMR (DMSO-d₆) 1.94 - 2.11 (m, 9 H), 2.22 (s, 3 H), 3.78 (d, 3 H), 5.46 (d, 2 H), 7.03 (s, 1 H), 7.18 (d, 3 H), 7.72 (br. s., 1 H), 7.86 (br. s., 1 H), 7.99 (d, 2 H), 8.26 (br. s., 1 H), 8.79 (d, 1 H), 9.76 (br. s., 1 H); MS (M+H⁺) = 441.

N-(2,4-dimethyl-5-pyridin-2-ylphenyl)-4-(pyridin-2-ylmethoxy)benzamide (34)

2.24 (d, 6 H), 5.34 (s, 2 H), 7.12 (d, 2 H), 7.26 (s, 1 H), 7.44 (s, 1 H), 7.54 (br. s., 1 H), 7.69 (d, 1 H), 7.88 - 8.01 (m, 3 H), 8.06

(s, 1 H), 8.40 (s, 1 H), 8.66 (d, 1 H), 8.80 (d, 1 H), 9.86 (s, 1 H); MS (M+H⁺) = 410.

N-(2,4-dimethyl-5-pyridin-3-ylphenyl)-4-(pyridin-2-ylmethoxy)benzamide

(35). ¹H NMR (DMSO-d₆) 2.20 (d, 6 H), 5.36 (s, 2 H), 7.12 (m, 2 H), 7.23 (s, 1 H), 7.31 (s, 1 H), 7.48 - 7.64 (m, 1 H), 7.72 (d, 1 H), 7.94 (m, 2 H), 8.01 (m, 1 H), 8.05 - 8.16 (m, 1 H), 8.48 (d, 1 H), 8.67 (d, 1 H), 8.77 - 8.94 (m, 2 H), 9.83 (s, 1 H); MS (M+H⁺) = 410.

N-[5-(5-aminopyridin-2-yl)-2,4-dimethylphenyl]-4-(pyridin-2-ylmethoxy)benzamide (36). ¹H NMR (DMSO-d₆) 2.21 (s, 6 H), 5.34 (s, 2 H), 7.12 (d, 2 H), 7.24 (s, 1 H), 7.34 (s, 1 H), 7.54 (d, 1 H), 7.60 - 7.75 (m, 3 H), 7.87 - 8.01 (m, 3 H), 8.06 (t, 1 H), 8.66 (d, 1 H), 9.84 (s, 1 H); MS (M+H⁺) = 425.

N-[5-(6-aminopyridin-2-yl)-2,4-dimethylphenyl]-4-(pyridin-2-ylmethoxy)benzamide (37). ¹H NMR (DMSO-d₆) 2.23 (d, 6 H), 5.40 (s, 2 H), 6.78 (d, 1 H), 6.95 (d, 1 H), 7.13 (d, 2 H), 7.18 - 7.29 (m, 1 H), 7.36 (s, 1 H), 7.52 - 7.70 (m, 1 H), 7.79 (d, 1 H), 7.85 - 8.00 (m, 3 H), 8.00 - 8.34 (m, 3 H), 8.71 (d, 1 H), 9.86 (s, 1 H), 14.06 (br. s., 1 H); MS (M+H⁺) = 425.

N-(5-(6-aminopyridazin-3-yl)-2,4-dimethylphenyl)-4-(pyridin-2-ylmethoxy)benzamide (38). ¹H NMR (DMSO-d₆) 2.23 (s, 3 H), 2.28 (s, 3 H), 5.28 (s, 2 H), 6.41 (s, 2 H), 6.83 (d, 1 H), 7.16 (m, 3 H), 7.31 (s, 1 H), 7.39 (m, 2 H), 7.54 (d, 1 H), 7.85 (m, 1 H), 7.96 (d, 2 H), 8.60 (m, 1 H), 9.76 (s, 1 H); MS (M+H⁺) = 426.

QM calculations: All QM calculations were performed using Jaguar,²² embedded within Schrodinger's Maestro package. Torsion profiles were generated using the relaxed coordinate scan protocol, using intervals of 10° between 0° and 360°. Calculations were performed at the DFT level theory, using the B3-LYP functional¹⁸ and a 6-31G** basis set.

Docking pose in SMO: The docking pose of 25 in SMO was generated using the Induced-Fit docking module²³ within Maestro, starting from the crystal structure of vismodegib in SMO (pdb 5L7I).¹²

AUTHOR INFORMATION

Corresponding Author

*Phone: +1 857-285-5304. E-mail: byang@kymeratx.com

Present Addresses

¹Department of Biochemistry and Molecular Biophysics, Washington University School of Medicine, 660 S. Euclid Avenue, Box 8231, St. Louis, MO 63110, United States.

[∞]Mersana Therapeutics Inc., 830 Memorial Drive, Cambridge, MD 02139, United States.

NOTES

The authors declare no competing financial interest.

ABBREVIATIONS USED

Hh, Hedgehog; SMO, Smoothed; QM, quantum mechanics; APCI, atmospheric pressure chemical ionization; ATP, adenosine 5-triphosphate; CDCl₃, deuterated chloroform; CI, chemical ionization; EI, electron impact; ESP, electrospray; iv, intravenous; LCMS, liquid chromatography-mass spectrometry; DMSO, dimethyl sulfoxide; PK, pharmacokinetics; PD, pharmacodynamics; EtOAc, ethyl acetate; DCM, dichloromethane; THF, tetrahydrofuran; MgSO₄, magnesium sulfate.

ASSOCIATED CONTENT

Supporting Information

The Supporting Information is available free of charge on the ACS Publications website at XXXXX.

In vivo PD results of compound **5** in Colo205 xenograft; QM based torsional scan results of compound **1**; Synthetic experimentals for compounds **28** and **29**; LC/MS and ¹H NMR spectras for compounds **25**, **26**, **33**, **35**, and **36**; assays protocols on solubility, LogD, rat microsome Clint, and hERG inhibition.

REFERENCE

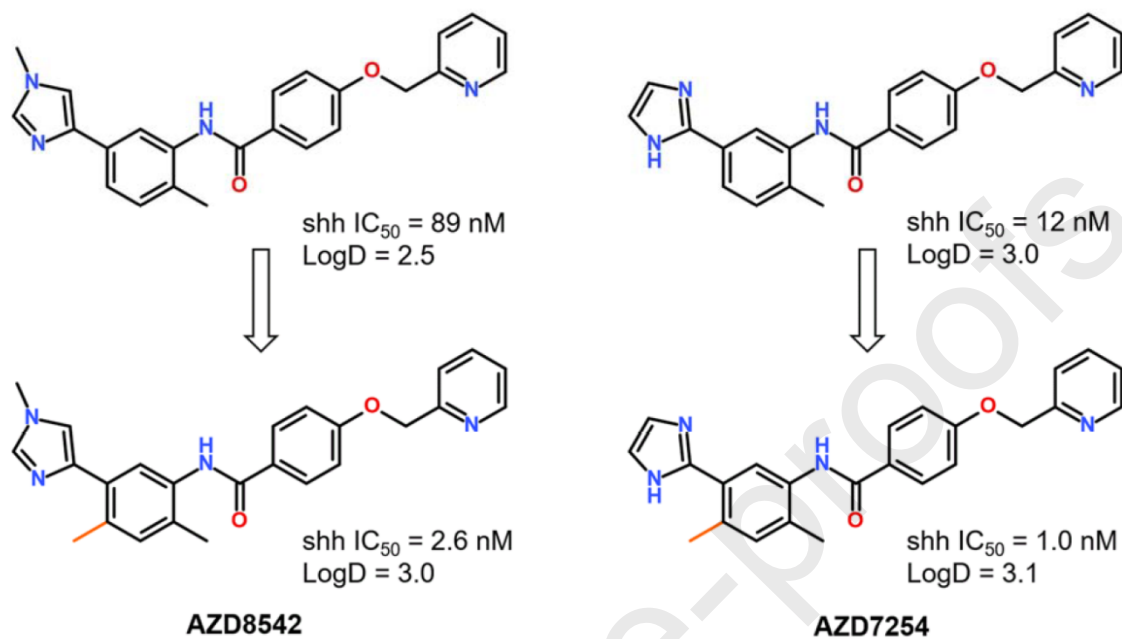
1. Ingham, P. W.; McMahon, A. P., Hedgehog signaling in animal development: paradigms and principles. *Genes Dev.* **2001**, *15* (23), 3059-3087.
2. Rubin, L. L.; de Sauvage, F. J., Targeting the Hedgehog pathway in cancer. *Nat. Rev. Drug Discovery* **2006**, *5* (12), 1026-1033.
3. Robarge, K. D.; Brunton, S. A.; Castanedo, G. M.; Cui, Y.; Dina, M. S.; Goldsmith, R.; Gould, S. E.; Guichert, O.; Gunzner, J. L.; Halladay, J.; Jia, W.; Khojasteh, C.; Koehler, M. F.; Kotkow, K.; La, H.; Lalonde, R. L.; Lau, K.; Lee, L.; Marshall, D.; Marsters, J. C., Jr.; Murray, L. J.; Qian, C.; Rubin, L. L.; Salphati, L.; Stanley, M. S.; Stibbard, J. H.; Sutherlin, D. P.; Ubhayaker, S.; Wang, S.; Wong, S.; Xie, M., GDC-0449 a potent inhibitor of the hedgehog pathway. *Bioorg. Med. Chem. Lett.* **2009**, *19* (19), 5576-81.
4. Pan, S.; Wu, X.; Jiang, J.; Gao, W.; Wan, Y.; Cheng, D.; Han, D.; Liu, J.; Englund, N. P.; Wang, Y.; Peukert, S.; Miller-Moslin, K.; Yuan, J.; Guo, R.; Matsumoto, M.; Vattay, A.; Jiang, Y.; Tsao, J.; Sun, F.; Pferdekamper, A. C.; Dodd, S.; Tuntland, T.; Maniara, W.; Kelleher, J. F., 3rd; Yao, Y. M.; Warmuth, M.; Williams, J.; Dorsch, M., Discovery of NVP- LDE225, a Potent and Selective Smoothened Antagonist. *ACS Med. Chem. Lett.* **2010**, *1* (3), 130-134.

5. Minami, Y.; Minami, H.; Miyamoto, T.; Yoshimoto, G.; Kobayashi, Y.; Munakata, W.; Onishi, Y.; Kobayashi, M.; Ikuta, M.; Chan, G.; Woolfson, A.; Ono, C.; Shaik, M. N.; Fujii, Y.; Zheng, X.; Naoe, T., Phase I study of glasdegib (PF-04449913), an oral smoothened inhibitor, in Japanese patients with select hematologic malignancies. *Cancer Sci.* **2017**, *108* (8), 1628-1633.
6. Munchhof, M. J.; Li, Q.; Shavnya, A.; Borzillo, G. V.; Boyden, T. L.; Jones, C. S.; LaGreca, S. D.; Martinez-Alsina, L.; Patel, N.; Pelletier, K.; Reiter, L. A.; Robbins, M. D.; Tkalcevic, G. T., Discovery of PF-04449913, a Potent and Orally Bioavailable Inhibitor of Smoothened. *ACS Med. Chem. Lett.* **2012**, *3* (2), 106-11.
7. Bendell, J.; Andre, V.; Ho, A.; Kudchadkar, R.; Migden, M.; Infante, J.; Tiu, R. V.; Pitou, C.; Tucker, T.; Brail, L.; Von Hoff, D., Phase I Study of LY2940680, a Smo Antagonist, in Patients with Advanced Cancer Including Treatment-Naive and Previously Treated Basal Cell Carcinoma. *Clin. Cancer Res.* **2018**, *24* (9), 2082-2091.
8. Gould, S. E.; Low, J. A.; Marsters, J. C., Jr.; Robarge, K.; Rubin, L. L.; de Sauvage F. J.; Sutherlin, D. P.; Wong, H.; Yauch, R. L., Discovery and preclinical development of vismodegib. *Expert Opin. Drug Discovery* **2014**, *9* (8), 969-984.
9. Jain, S.; Song, R.; Xie, J., Sonidegib: mechanism of action, pharmacology, and clinical utility for advanced basal cell carcinomas. *OncoTargets Ther.* **2017**, *10*, 1645-1653.
10. Weierstall, U.; James, D.; Wang, C.; White, T. A.; Wang, D.; Liu, W.; Spence, J. C.; Bruce Doak, R.; Nelson, G.; Fromme, P.; Fromme, R.; Grotjohann, I.; Kupitz, C.; Zatsepin, N. A.; Liu, H.; Basu, S.; Wacker, D.; Han, G. W.; Katritch, V.; Boutet, S.; Messerschmidt, M.; Williams, G. J.; Koglin, J. E.; Marvin Seibert, M.; Klinker, M.; Gati, C.; Shoeman, R. L.; Barty, A.; Chapman, H. N.; Kirian, R. A.; Beyerlein, K. R.; Stevens, R. C.; Li, D.; Shah, S. T.; Howe, N.; Caffrey, M.; Cherezov, V., Lipidic cubic phase injector facilitates membrane protein serial femtosecond crystallography. *Nat. Commun.* **2014**, *5*, 3309.
11. Wang, C.; Wu, H.; Evron, T.; Vardy, E.; Han, G. W.; Huang, X. P.; Hufeisen, S. J.; Mangano, T. J.; Urban, D. J.; Katritch, V.; Cherezov, V.; Caron, M. G.; Roth, B. L.; Stevens, R. C., Structural

- basis for Smoothed receptor modulation and chemoresistance to anticancer drugs. *Nat. Commun.* **2014**, *5*, 4355.
12. Byrne, E. F. X.; Sircar, R.; Miller, P. S.; Hedger, G.; Luchetti, G.; Nachtergaele, S.; Tully, M. D.; Mydock-McGrane, L.; Covey, D. F.; Rambo, R. P.; Sansom, M. S. P.; Newstead, S.; Rohatgi, R.; Siebold, C., Structural basis of Smoothed regulation by its extracellular domains. *Nature* **2016**, *535* (7613), 517-522.
 13. Huang, P.; Zheng, S.; Wierbowski, B. M.; Kim, Y.; Nedelcu, D.; Aravena, L.; Liu, J.; Kruse, A. C.; Salic, A., Structural Basis of Smoothed Activation in Hedgehog Signaling. *Cell* **2018**, *174* (2), 312-324 e16.
 14. Yang, B.; Hird, A. W.; Russell, D. J.; Fauber, B. P.; Dakin, L. A.; Zheng, X.; Su, Q.; Godin, R.; Brassil, P.; Devereaux, E.; Janetka, J. W., Discovery of novel hedgehog antagonists from cell-based screening: Isosteric modification of p38 bisamides as potent inhibitors of SMO. *Bioorg. Med. Chem. Lett.* **2012**, *22* (14), 4907-11.
 15. Yauch, R. L.; Gould, S. E.; Scales, S. J.; Tang, T.; Tian, H.; Ahn, C. P.; Marshall, D.; Fu, L.; Januario, T.; Kallop, D.; Nannini-Pepe, M.; Kotkow, K.; Marsters, J. C.; Rubin, L. L.; de Sauvage, F. J., A paracrine requirement for hedgehog signalling in cancer. *Nature* **2008**, *455* (7211), 406-410.
 16. Hwang, R. F.; Moore, T. T.; Hattersley, M. M.; Scarpitti, M.; Yang, B.; Devereaux, E.; Ramachandran, V.; Arumugam, T.; Ji, B.; Logsdon, C. D.; Brown, J. L.; Godin, R., Inhibition of the hedgehog pathway targets the tumor-associated stroma in pancreatic cancer. *Mol. Cancer Res.* **2012**, *10* (9), 1147-1157.
 17. Levy, G. C. H., T.; Stelgel, A., Intra- and intermolecular hydrogen bonding in chlorinated phenols and related compounds. *J. Phys. Chem.* **1975**, *79* (21), 2325-2327.
 18. Becke, A. D., Density-functional thermochemistry. III. The role of exact exchange. *J. Chem. Phys.* **1993**, *98* (7), 5648-5652.

19. Patani, G. A.; LaVoie, E. J., Bioisosterism: A Rational Approach in Drug Design. *Chem. Rev.* **1996**, *96* (8), 3147-3176.
20. Giannetti, A. M.; Wong, H.; Dijkgraaf, G. J.; Dueber, E. C.; Ortwine, D. F.; Bravo, B. J.; Gould, S. E.; Plise, E. G.; Lum, B. L.; Malhi, V.; Graham, R. A., Identification, characterization, and implications of species-dependent plasma protein binding for the oral Hedgehog pathway inhibitor vismodegib (GDC-0449). *J. Med. Chem.* **2011**, *54* (8), 2592-2601.
21. Leung, C. S.; Leung, S. S.; Tirado-Rives, J.; Jorgensen, W. L., Methyl effects on protein-ligand binding. *J. Med. Chem.* **2012**, *55* (9), 4489-4500.
22. Bochevarov, A. D.; Harder, E.; Hughes, T. F.; Greenwood, J. R.; Braden, D. A.; Philipp, D. M.; Rinaldo, D.; Halls, M. D.; Zhang, J.; Friesner, R. A., Jaguar: A high-performance quantum chemistry software program with strengths in life and materials sciences. *Int. J. Quantum Chem.* **2013**, *113* (18), 2110-2142.
23. Sherman, W.; Beard, H. S.; Farid, R., Use of an induced fit receptor structure in virtual screening. *Chem. Biol. Drug Des.* **2006**, *67* (1), 83-84.

TABLE OF CONTENTS GRAPHIC



Conflict of Interest

The authors are current or former employees of AstraZeneca PLC.

Journal Pre-proofs